Online Resource 1

Kandil Concrete-Faced Rockfill Dam and its Response to the 2023 Kahramanmaraş Earthquake Sequence from Strong-Motion Records, Instrumentation, and Underwater Inspection

Murat Eröz, Enerjisa Üretim A.Ş., Asset Management and Sustainability Directorate, Istanbul, Türkiye. Email: murat.eroz@enerjisauretim.com. Natural Hazards

This Online Resource contains the methods and sensitivity notes (Text S1), the supporting figures (Figs. S1 to S9), and the tables (Tables S1 to S10) cited in the main text.

Text S1. Methods and sensitivity notes

S1.1 Processing of the strong-motion records. The raw records (100 samples per second) were demeaned, tapered, and band-pass filtered between 0.1 and 25 Hz with a fourth-order zero-phase Butterworth filter. The horizontal components were rotated by 29° from north into the primary (upstream to downstream) and secondary (dam axis) directions; the crest axis determined from the 12 parapet survey points lies at 121° from north, so that the primary direction is 31°, and the 2° difference changes the peak values by less than 1%. Peak accelerations in Table 4 of the main text are the absolute maxima of the baseline-corrected records before band-pass filtering. Response spectra (5% damping) were computed by Newmark average-acceleration integration of the single-degree-of-freedom equation at a time step of 0.002 s and verified against a fourth-order Runge–Kutta solution and against an independent computation. Fourier amplitude ratios were smoothed with the Konno and Ohmachi (1998) window ($b = 40$). Equivalent damping was estimated from the half-power bandwidth of the smoothed crest-to-abutment ratio around its peak. For the Elbistan event the peak at 2.27 Hz is broad and overlaps the pre-event mode at 2.6 to 3.2 Hz, so that the bandwidth gives 32% with the full band and 20% with the upper half-power frequency taken at the intervening minimum; both are upper bounds of the equivalent damping and the paper reports 20 to 30%. The reference spectral shape is the elastic design spectrum of DBYBHY 2007 (Ministry of

Public Works and Settlement 2007) for local site class Z1 (rock), $S(T) = 1 + 1.5T/T_A$ for $T \le T_A$, 2.5 for $T_A < T \le T_B$, and $2.5(T_B/T)^{0.8}$ for $T > T_B$, with $T_A = 0.10$ s and $T_B = 0.30$ s, multiplied by the MCE PGA of 0.45 g; it is a reference for the level of the design input, not the design spectrum. The design accelerogram is the record of AFAD station 0105 (Adana Ceyhan Tarım İlçe Müdürlüğü, V_{s30} 263 m/s) for the earthquake of June 27, 1998, as processed in the Engineering Strong Motion database (Luzi et al. 2020) with baseline removal and a second-order Butterworth band-pass of 0.025 to 40 Hz; the EW and NS components have peak accelerations of 276 and 221 cm/s^2, peak velocities of 24 and 30 cm/s, and mean periods of 0.64 and 0.74 s, and each was scaled linearly to 0.45 g. A fourth-order low-pass filter at 10 or 15 Hz, applied to represent the high-frequency filtering of the design, changes the scaled ordinates at periods of 0.2 s and longer by less than 3%, and by up to 13% at 0.1 s for the 10 Hz filter.

S1.2 Relative displacement and apparent shear strain. The crest and abutment records were aligned by cross-correlation of their long-period displacement traces (lag 0.38 s, correlation 0.90 for the north component), doubly integrated, and band-pass filtered between 0.2 and 8 Hz. The apparent average shear strain is the peak crest-minus-abutment displacement divided by the dam height of 103 m, and the effective strain is 0.65 times the peak (Seed and Idriss 1971). A time-base error of ±0.3 s changes the peak relative displacement of the Elbistan record by less than 10%, and a 0.2 to 5 Hz band gives 6.5 cm instead of 7.3 cm.

S1.3 Modulus reduction curves. The curves of Menq (2003) for gravelly soils are $G/G_{max} = 1/[1 + (\gamma/\gamma_r)^a]$ with $\gamma_r = 0.12\, C_u^{-0.6}\, (\sigma'_0/p_a)^n$ in percent, $n = 0.5\, C_u^{-0.15}$, and $a = 0.86 + 0.1 \log_{10}(\sigma'_0/p_a)$, where C_u is the coefficient of uniformity, σ'_0 the mean effective confining stress, and p_a the atmospheric pressure. For C_u between 10 and 50 and σ'_0 between 400 and 1000 kPa, G/G_{max} is 0.25 to 0.65 at

strains of 0.03 to 0.06% (Elbistan) and 0.45 to 0.95 at 0.004 to 0.02% (Pazarcık); the ratio for matched C_u and σ'_0 is 0.45 to 0.70. The period-based ratio is $(0.34/0.44)^2 = 0.60$.

S1.4 Sliding block calculations. The Newmark (1965) rigid block was integrated for one-directional sliding with the yield acceleration $k_y g$ applied to both polarities of the band-passed primary-direction records. The Bray and Travasarou (2007) procedure was applied with $T_s = 0.34$ s, $S_a(1.5T_s) = 0.40$ g from the abutment spectrum, and Mw 7.6; the probability of negligible displacement is $P = 1 - \Phi(-1.76 - 3.22 \ln k_y - 0.484\, T_s \ln k_y + 3.52 \ln S_a)$, which gives 0.40 at $k_y = 0.21$, and the conditional median follows the non-zero displacement equation of the method with its standard deviation of 0.66. The rigid form of the procedure used the PGA of the baseline-corrected abutment record, 0.718 g (0.75 g for the band-passed record, which gives 18 cm instead of 17 cm). The reduction of the average acceleration of a sliding mass extending to about a quarter of the height was taken as 0.8 of the crest value after Makdisi and Seed (1978). The upper shell yield coefficient was estimated from the infinite slope relation $k_y = \tan(\varphi - \beta)$ with $\beta = 35.5°$ for the 1.4H to 1V slope and φ of 46° to 52° for rockfill at normal stresses of 50 to 150 kPa (Leps 1970). Linear extrapolation of the pseudo-static factors of safety of the design (1.105 at $k = 0.18$ and 1.067 at $k = 0.20$) to unity gives $k = 0.235$. The positive primary direction of the processed records points toward the reservoir (azimuth 29°), so that downstream sliding of a block on the downstream slope occurs when the primary acceleration exceeds $k_y g$ in the positive sense; the block accelerates relative to the ground while the ground acceleration exceeds the yield value, decelerates afterwards, and stops when its relative velocity returns to zero, and sliding is one-directional (no upslope movement). The values in Table 6 of the main text are given for this polarity; the opposite polarity is reported in parentheses as a sensitivity case. The average acceleration of the sliding mass was taken as 0.8 of the crest record for a mass extending to a quarter of the height, 0.65 for 0.4 of

the height, and 0.35 for the full height, following the ratio of maximum average acceleration to maximum crest acceleration of Makdisi and Seed (1978); scaling the whole record by one factor neglects the change in frequency content with depth. The effect of the vertical acceleration was bounded by integrating with a time-varying yield coefficient $k_y(t) = k_y(1 + a_v(t)/g)$, with a_v the vertical crest acceleration scaled by the same factor as the horizontal record, taken with both signs; the displacements change by less than 10% (for example 32.0 cm against 32.9 and 32.0 cm at k_y = 0.20 for the quarter-height mass).

S1.5 Foundation pore pressures. The excess head of each piezometer is defined relative to a linear regression of its head on the reservoir level fitted to the daily readings from January 15 to February 5, 2023 (slopes 0.55 to 1.04, residual standard deviations below 0.1 m). The decay after the events was fitted by $h(t) = A \exp(-t/\tau) + C$ to the 20-min readings from February 6, 17:10, to March 20, 2023, with t measured from the Elbistan earthquake (13:24); the e-folding times τ are 16, 19, 19, and 10 h for VWP1, VWP2, VWP3, and VWP8, the coefficients of determination 0.98 to 0.99, and the constant C is the persistent offset. Fits restricted to the first three days give e-folding times of 13 to 29 h and peaks at 13:24 of 9, 16, 22, and 7 m, which define the upper values of the ranges quoted in the main text. If the rise is assigned to the Pazarcık earthquake (04:17) instead, the extrapolated peaks increase by 40 to 60% and the e-folding times by about 30%. The hydraulic diffusivity was estimated as $D = z^2/(0.91\ t_{50})$, the time for the excess pressure at depth z below a drained boundary to fall to half of a uniform initial value in a semi-infinite medium, with z the depth of the sensor below the plinth and t_{50} the measured half-time of the transient part; with a specific storage of 10^{-6} to 10^{-5} m^{-1} this corresponds to hydraulic conductivities of about 10^{-9} to 5×10^{-7} m/s, that is 0.01 to 4 Lugeon; both quantities are illustrative because the drainage length is unknown and the diffusivity scales with its square.

S1.6 Surface survey. The 12 parapet points and 22 downstream surface points are observed by total station from reference pillars on the abutments; the coordinates before and after the earthquakes are those of the surveys of August 4, 2022 and February 8, 2023 for 31 points and of the dates listed in Table S9 for SF3, SF13, and SF15. The displacement vectors were rotated into the dam axis system defined by the least-squares line through the parapet points (azimuth 121°), with the downstream direction at 211°. The fraction of the displacement developed above El. 1060 m quoted in Section 5.4 of the main text is defined for each section as $(d_{top} - d_{1060})/d_{top}$, where d_{top} is the downstream displacement of the crest edge or El. 1076 m point and d_{1060} that of the El. 1060 m point in the same section (Table S9); it is 0.71 and 0.77 for the centre and right-of-centre sections (SF12 and SF14, SF1 and SF3), 0.63, 0.51, and 0.32 for the sections 12, 37, and 62 m left of centre, and it describes the surface profile only.

Supplementary figures

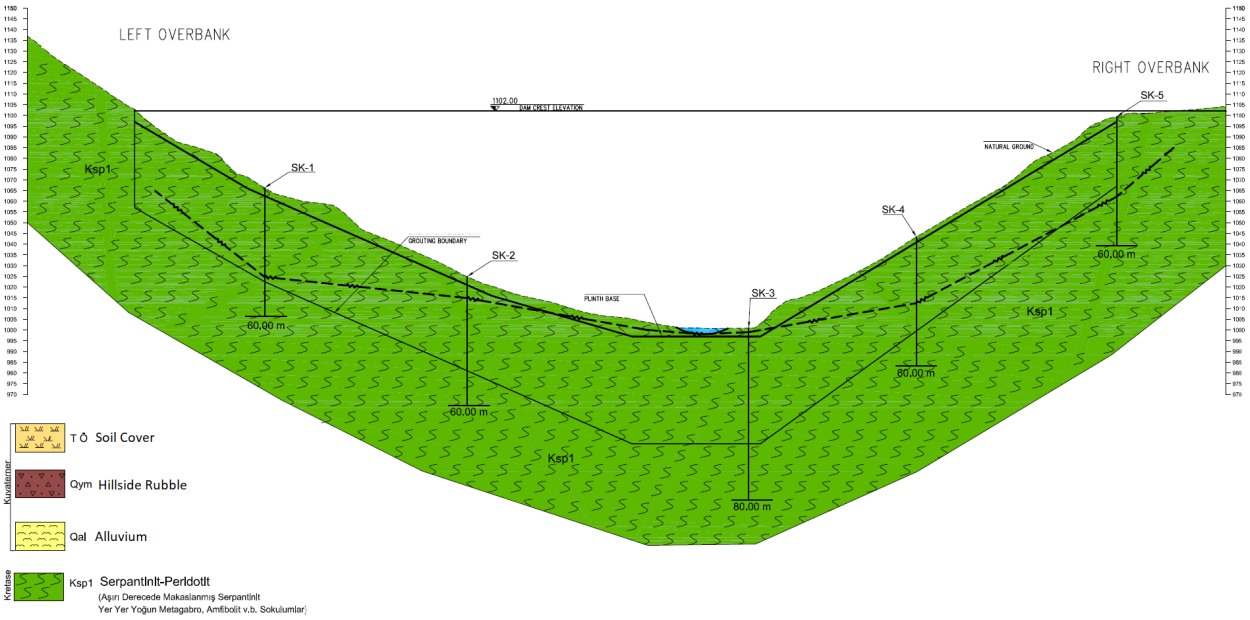
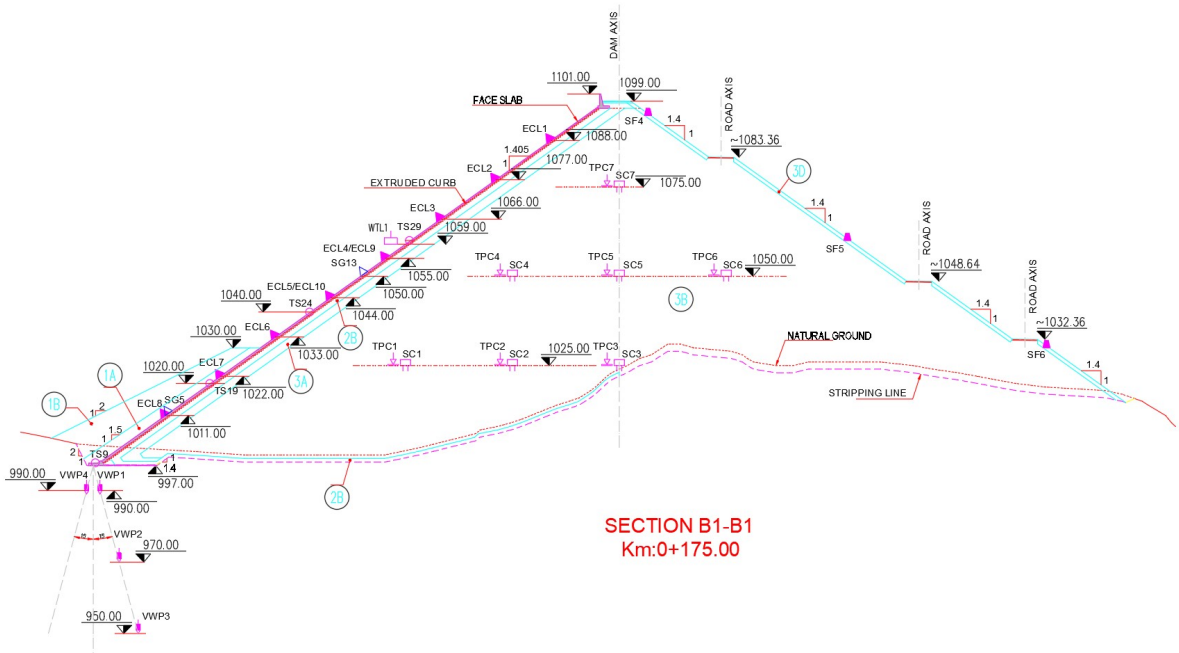


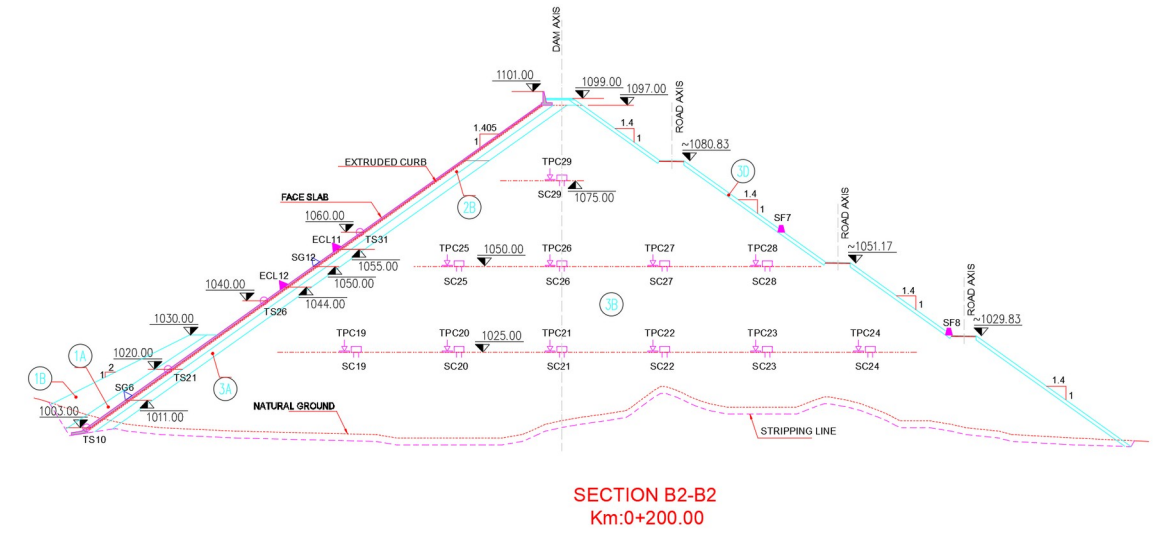
Fig. S1 Geological section of dam site



109

110 **Fig. S2** Instrument locations in Section B1-B1

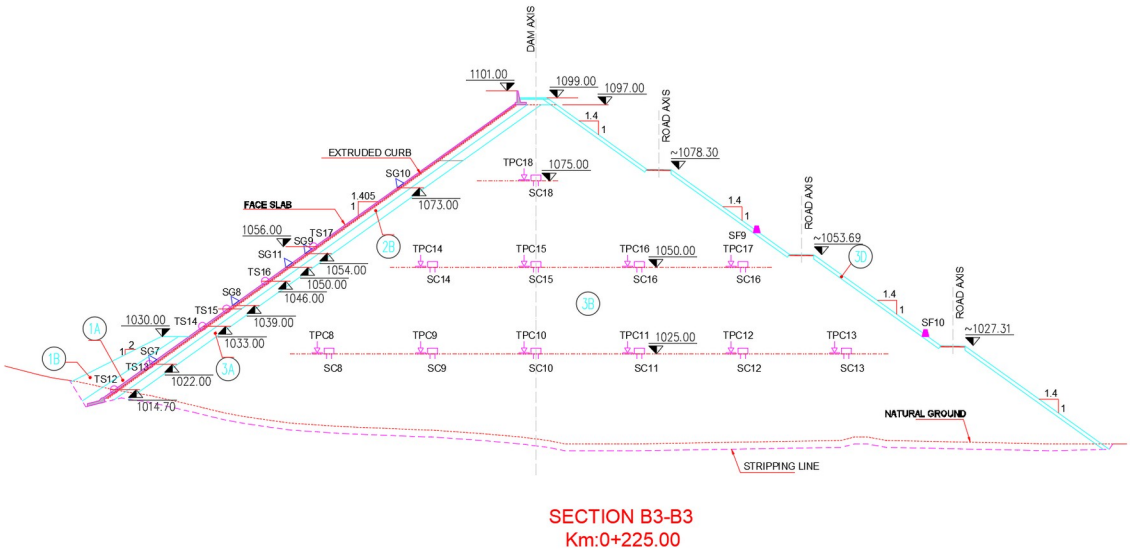
111



112

113 **Fig. S3** Instrument locations in Section B2-B2

114



115

116 **Fig. S4** Instrument locations in Section B3-B3

117

EQUIPMENT LIST				
NO	NAME	SHORTENING	SCHEME	QUANTITY
1	TOTAL EARTH PRESSURE CELL	TPC		29
2	VIBRATING WIRE PIEZOMETER	VWP		12
3	HYDRAULIC OR ELECTR?C SETTLEMENT CELL	SC		29
4	WATER LEVEL METER	WTL		1
5	SURFACE MONUMENT	SF		15
6	JOINTMETER	HJM		12
7	JOINTMETER	PJM		11
8	INSTRUMENTATIONAL TERMINAL	AMR		1
9	REFERENCE MONUMENT	SRR		2
10	ELECTROLEVEL	ECL		12
11	STRAIN GAUGE	SG		15
12	TEMPERATURE SENSOR	TS		32
13	ACCELEROMETER	AC		2

118

119 **Fig. S5** Equipment list and scheme



Fig. S6 Rockfalls on right abutment slopes



Fig. S7 Location of V-notch weir structure



Fig. S8 Weathering crack in the PVC cover above the reservoir level



Fig. S9 Underwater ROV used in dam inspection

Supplementary tables

Table S1 Gradation limits for the 2A peripheral joint filter zone

Sieve Metric AS Aperture (mm)	Limits of Percentage Passing Sieve Aperture by Mass
38.10	100
19.10	85–100
4.76	50–75
1.19	25–50
0.297	10–25
0.074	0–5

Table S2 Gradation limits for the 2B cushion zone

Sieve Metric AS Aperture (mm)	Limits of Percentage Passing Sieve Aperture by Mass
76.20	100
38.10	70–100
19.10	55–80
4.76	35–60
1.19	18–40
0.297	6–18
0.074	0–7 (cohesionless)

Table S3 Quality control tests for materials to be placed in dam zones (before backfilling)

Experiment	**Standard**
Grain size distribution	ASTM D-422
Specific gravity	ASTM C-127
Los Angeles experiment (Grading 4)	ASTM C-131
Sodium-sulphate resistance test	ASTM C-88
Relative density	ASTM D-2049

Table S4 Tests conducted during body construction

Experiment	**Standard**
Grain size distribution	ASTM D-422
Los Angeles experiment (Grading 4)	ASTM C-131
Sodium-sulphate resistance test	ASTM C-88
Load bearing capacity test	DIN 18134

Table S5 Safety coefficients used in sliding analysis

	Dam Body
End of Construction	>1.5
End of Construction (OBE)	>1.0
Operation	>1.5
Operation (OBE)	>1.2
Operation (MCE)	>1.0

Table S6 AFAD calculated parameters for Pazarcık earthquake (Mw: 7.7), band-pass filtered records (Butterworth, 0.1 to 25 Hz) (AFAD 2023)

Station	PGA (cm/s^2)	PGV (cm/s)	PGD (cm)	Significant Duration (s)	Bracketed Duration (s)
4614 Kahramanmaraş Pazarcık	2156.8	74	30.8	23.9	61.6
Narlı (NAR)	597	87	44	42.5	64
4615 Narlı	535.8	115	80.2	47.4	68
4616 Türkoğlu	641.4	108.6	41.6	41.7	68.6

Table S7 AFAD calculated parameters for Elbistan earthquake (Mw: 7.6), band-pass filtered records (Butterworth, 0.1 to 25 Hz) (AFAD 2023)

Station	PGA (cm/s^2)	PGV (cm/s)	PGD (cm)	Significant Duration (s)	Bracketed Duration (s)
4612 Kahramanmaraş Göksun	691.1	115.7	66.5	28.7	74
4611 Çağlayancerit	206.3	30.7	27	35.3	70
4406 Malatya Akçadağı	445.2	27.7	15.2	18.4	43
4631 Kahramanmaraş Nurhak	356.2	70.9	45.7	26.8	69.65

Table S8 Dam-body instrument list

Instrument	Quantity	Location	Status
Reservoir water level (RLG)	1	Upstream face	All functional
Total pressure cell (TPC)	29	Dam body	All functional
Settlement cell (SC)	29	Dam body	All functional
Vibrating wire piezometer (VWP)	12	Dam foundation and abutments	1 dysfunctional
Strain gauge (SG)	$15 \times 2 = 30$	Upstream face	13 (9 *x*-axis, 4 *y*-axis) components dysfunctional

One-dimensional hydraulic joint meter (HJM)	12	Face-slab joints	7 dysfunctional
Three-dimensional pendulum joint meter (PJM)	$11 \times 3 = 33$	Plinth-slab joints	9 (5 *x*-axis, 2 *y*-axis, 2 *z*-axis) components dysfunctional
Electro level meter (ECL)	12	Upstream face	All functional
Temperature sensor (TS)	32	Upstream face	7 dysfunctional
V-notch weir (VN)	1	Downstream	All functional
Topographic measurement (SF)	34	Crest and downstream face	All functional
Accelerometer (AC)	2	Dam-body crest and foundation	All functional

Table S9 Displacements of the parapet points (D1 to D12) and the downstream surface points (SF1 to SF22) between the surveys before and after the earthquakes, in the dam axis system

Point	Elevation (m)	Along the axis (m)	Downstream of the parapet (m)	Survey before	Survey after	Downstream (cm)	Toward left abutment (cm)	Vertical (cm)
D1	1099.8	-160	0.0	2022-08-04	2023-02-08	+2.5	+3.4	-0.8
D2	1099.7	-134	0.0	2022-08-04	2023-02-08	+4.3	+3.2	-3.4
D3	1099.7	-104	0.0	2022-08-04	2023-02-08	+5.2	+3.5	+2.0
D4	1099.6	-75	0.1	2022-08-04	2023-02-08	+6.6	+3.8	+0.7
D5	1099.6	-45	0.1	2022-08-04	2023-02-08	+7.6	+4.6	-0.6
D6	1099.6	-14	0.1	2022-08-04	2023-02-08	+7.6	+5.5	-1.3
D7	1099.7	+18	0.0	2022-08-04	2023-02-08	+7.0	+6.8	-0.4
D8	1099.7	+43	0.0	2022-08-04	2023-02-08	+6.8	+7.2	-6.2
D9	1099.7	+73	0.0	2022-08-04	2023-02-08	+6.2	+7.8	-5.4
D10	1099.8	+105	0.0	2022-08-04	2023-02-08	+5.4	+8.8	-3.5
D11	1099.7	+132	0.0	2022-08-04	2023-02-08	+4.1	+8.1	-2.0
D12	1099.8	+159	0.0	2022-08-04	2023-02-08	+3.8	+8.4	-1.1
SF1	1096.2	+64	12.5	2022-08-04	2023-02-08	+37.9	+10.0	-12.1
SF2	1092.7	+113	24.1	2022-08-04	2023-02-08	+26.1	+11.8	-8.0
SF3	1059.2	+65	71.1	2022-08-04	2023-03-02	+8.7	+6.3	+1.5
SF4	1095.2	+13	13.6	2022-08-	2023-02-	+25.2	+12.3	-8.9

Point	Elevation (m)	Along the axis (m)	Downstream of the parapet (m)	Survey before	Survey after	Downstream (cm)	Toward left abutment (cm)	Vertical (cm)
				04	08			
SF5	1095.7	-62	13.2	2022-08-04	2023-02-08	+12.5	+3.0	-4.1
SF6	1095.6	-136	13.5	2022-08-04	2023-02-08	+7.5	+4.1	+0.0
SF7	1075.5	-138	41.2	2022-08-04	2023-02-08	+4.1	+3.3	+4.1
SF8	1075.9	-97	40.7	2022-08-04	2023-02-08	+6.3	+2.8	+1.4
SF9	1075.9	-61	47.8	2022-08-04	2023-02-08	+13.1	+0.6	-6.5
SF10	1075.9	-37	47.5	2022-08-04	2023-02-08	+18.8	+5.1	-10.5
SF11	1076.2	-11	47.0	2022-08-04	2023-02-08	+25.0	+4.9	-11.3
SF12	1076.1	+15	47.1	2022-08-04	2023-02-08	+38.9	+7.3	-11.1
SF13	1076.6	+65	46.9	2020-09-07	2023-03-02	+14.0	+6.2	-3.2
SF14	1060.0	+13	69.7	2022-08-04	2023-02-08	+11.2	+6.3	-1.2
SF15	1059.5	-12	70.1	2021-06-04	2023-03-02	+9.2	+3.5	-0.5
SF16	1059.6	-38	70.5	2022-08-04	2023-02-08	+9.3	+4.6	-1.3
SF17	1060.4	-63	69.1	2022-08-04	2023-02-08	+8.8	+3.8	-0.7
SF18	1061.8	-98	67.3	2022-08-04	2023-02-08	+5.4	+3.4	+2.2
SF19	1031.2	+13	124.5	2022-08-04	2023-02-08	+6.2	+6.0	+3.1
SF20	1030.7	-12	117.9	2022-08-04	2023-02-08	+7.0	+5.0	+2.4
SF21	1030.5	-37	118.4	2022-08-04	2023-02-08	+6.5	+4.4	+2.9
SF22	1030.4	-63	118.3	2022-08-04	2023-02-08	+5.1	+3.9	+3.7

Along the axis positive toward the right abutment; downstream distance measured from the line of the parapet survey points at the crest; displacements in cm, downstream and toward the left abutment positive, vertical positive upward. The crest axis azimuth from the parapet points is 121°, the downstream direction 211°. Three points (SF3, SF13, SF15) bracket longer intervals as listed. The network is observed by total station from reference pillars on the abutment rock; the along-axis component shared by all points is attributed to a shift of the pillars and does not affect the downstream profile (Section 5.4 of the main text)

Table S10 Leakage and remedial treatment at selected CFRDs (after ICOLD 2010)

Dam	Country	Year Completed	Height (m)	Rock Type	Initial Leakage (l/s)	Remedial Treatment
Turimiquire	Venezuela	1987	115	Limestone	6000	Yes
Alto Anchicaya	Colombia	1974	140	Hornfels–diorite	1800	Yes
Shiroro	Nigeria	1984	125	Granite	1800	Yes
Ita	Brazil	2000	125	Basalt	1700	Yes
Golillas	Colombia	1984	125	Gravel	1080	Yes
Segredo	Brazil	1993	140	Basalt	400	Yes
Minase	Japan	1963	67	Liparite	400	Yes
Aguamilpa	Mexico	1993	187	Gravel	260	Yes
Foz do Areia	Brazil	1980	160	Basalt	236	Yes
Xingo	Brazil	1994	140	Granite	160–200	Yes
Tianshengqiao	China	1999	178	Limestone and mudstone	100	No
Salvajina	Colombia	1984	148	Gravel	60	No
Chengbing	China	1989	75	Lava tuff	60	No
Khao Laem	Thailand	1984	130	Limestone	53	Yes
Crotty	Australia	1991	83	Gravel	38	No
Mackintosh	Australia	1981	75	Graywacke	14	No
Pichi-Picun-Leufu	Argentina	1999	40	Gravel	13	No
Cethana	Australia	1971	110	Quartzite	7	No
Murchison	Australia	1982	89	Rhyolite	7	No
Bastyan	Australia	1983	75	Graywacke	2	No

References cited in this supplement

Bray JD, Travasarou T (2007) Simplified procedure for estimating earthquake-induced deviatoric slope displacements. J Geotech Geoenviron Eng 133:381–392

Disaster and Emergency Management Authority (AFAD) (2023) February 6, 2023 Mw 7.7 Pazarcık and Mw 7.6 Elbistan-Kahramanmaraş earthquakes: Earthquake Information Support System (DeBiDeS). AFAD, Ankara, Türkiye

International Commission on Large Dams (ICOLD) (2010) Concrete face rockfill dams: concepts for design and construction. Bulletin 141. ICOLD, Paris

Konno K, Ohmachi T (1998) Ground-motion characteristics estimated from spectral ratio between horizontal and vertical components of microtremor. Bull Seismol Soc Am 88:228–241

Leps TM (1970) Review of shearing strength of rockfill. J Soil Mech Found Div 96:1159–1170

Luzi L, Lanzano G, Felicetta C, D'Amico MC, Russo E, Sgobba S, Pacor F, ORFEUS Working Group 5 (2020) Engineering Strong Motion Database (ESM), version 2.0. Istituto Nazionale di Geofisica e Vulcanologia. https://doi.org/10.13127/ESM.2

Makdisi FI, Seed HB (1978) Simplified procedure for estimating dam and embankment earthquake-induced deformations. J Geotech Eng Div 104:849–867

Menq FY (2003) Dynamic properties of sandy and gravelly soils. PhD dissertation, The University of Texas at Austin

Ministry of Public Works and Settlement (2007) Specification for buildings to be built in seismic zones (DBYBHY 2007). Official Gazette No. 26454, 6 March 2007, Ankara, Türkiye

Newmark NM (1965) Effects of earthquakes on dams and embankments. Géotechnique 15:139–160

Seed HB, Idriss IM (1971) Simplified procedure for evaluating soil liquefaction potential. J Soil Mech Found Div 97:1249–1273